

Supplementary Information:

Broad-spectrum antibacterial hydrogel based on the synergistic action of Fmoc-phenylalanine and Fmoc-lysine in a co-assembled state

Bodhisattwa Das Gupta[†], Arpita Halder[†], Thangavel Vijayakanth[‡], Nandita Ghosh[†], Ranik Konar[†], Oindrilla Mukherjee[†], Ehud Gazit^{‡}, Sudipta Mondal^{†*}*

[†]Department of Biotechnology, National Institute of Technology, Durgapur, 713209, India

[‡] The Shmunis School of Biomedicine and Cancer Research George S. Wise Faculty of Life Sciences, Tel Aviv University, Tel Aviv 6997801, Israel; Department of Materials Science and Engineering Iby and Aladar Fleischman Faculty of Engineering, Tel Aviv University, Tel Aviv 6997801, Israel

Correspondence to: sudipta.mondal@bt.nitdgp.ac.in; EhudGa@tauex.tau.ac.il

Table of Contents

Figure S1. (a) Digital image of 10 mM Fmoc-K in 100 mM PB (b) Evaluation of the impact of Fmoc-K on the development of *E. coli* by turbidity measurement (absorbance values at 600 nm).

Figure S2. (a) Composition of Fmoc-K with varying concentrations of Fmoc-F (M1, M2, M3, M4, M5, M6 and M7). (b) Growth inhibition kinetics reflecting the effect of Fmoc-K with variable Fmoc-F concentrations on *E. coli*. (c) Effect of (M1 to M7) on *S. aureus* growth.

Figure S3. Effect of P1 and their components (Fmoc-F and Fmoc-K) on the Gram-positive bacterial membrane.

Figure S4. (a) Merged Fluorescence image (Blue fluorescence for DAPI and red fluorescence for PI) before and after treatment of *E. coli* with P1 (b) percentage cell death by counting the number of dead bacterial cells using ImageJ.

Figure S5. (a) Strain sweep tests at a constant applied frequency (0.1 Hz) for the self-assembled Fmoc-F and co-assembled composite gels P1 (b), P2 (c) and P3 (d) validate a broad linear viscoelastic regime (LVR).

Figure S6. Fluorescence spectra of Fmoc-F, P1, P2 and P3.

Figure S7. Distribution of sizes of the different clusters (number of atoms present in each cluster) and their frequencies as observed in MD simulation.

Figure S8. Snapshot of (a) π - π interaction and H-bonding/salt-bridge formation between Fmoc-K and Fmoc-F as observed in simulation. (b), (c), (d) π - π interaction and H-bonding between different molecules of Fmoc-F as observed in simulation.

Figure S9. Snapshot of (a) a cluster and (b) a fibre lattice formed by the interactions between different molecules of Fmoc-F and Fmoc-K as observed at the final time frame of the simulation.

Figure S10. (a) Variation of solvent accessible surface area (SASA) of Fmoc-F (blue) and Fmoc-K (red) and co-assembled system (black) with simulation time. Convergence of SASA indicates a stable co-assembled system. (b) Variation of number of clusters as a function of simulation time. (c) Evolution of the number of H-bonds observed in the simulation process. The blue curve represents the H-bonding interaction between the amino acid conjugates and salts and waters present in the system. The red curve represents intermolecular and intramolecular H-bonding between Fmoc-K and Fmoc-F.

1. Experimental Section

MD simulation: The molecular dynamic simulation was performed in GROMACS 2023.4 using OPLS-AA force field.¹⁻³ The models of Fmoc-F and Fmoc-K was prepared by the builder program in pymol.^{4,5} As the parameters for Fmoc group was not available in default OPLS-AA, the Fmoc parameters optimized by Ren and co-worker was included in the force field file.⁶ Two different systems were prepared. In the first system 100 Fmoc-F and 50 Fmoc-K molecules was inserted in a cubic box having a dimension of 13.25 nm × 13.25 nm × 13.25 nm. In the second system, same number of molecules were placed in a cubic box of 8 nm × 8 nm × 8 nm. The systems were solvated with TIP3P water and energy minimized to remove high-energy contacts.⁷ Following this, the system was equilibrated under NVT and NPT conditions at 300K and 1 bar for 100 ps, respectively in which the heavy atoms were position restrained. The production MD run was performed for a total of 650 ns with first system and 500 ns with the second system in which LINCS constraint algorithm was used to constrain the bonds and PME was employed for long-range electrostatic with a non-bonded interactions cut-off of 1 nm. Velocity rescaling algorithms have been used to control the system temperature and pressure in the system was maintained with Parrinello-Rahman barostat.^{8,9} MD run was performed with leap-frog integrator with a step size of 2 fs.¹⁰ The inbuilt GROMACS tools have been utilized for the post-MD analysis.

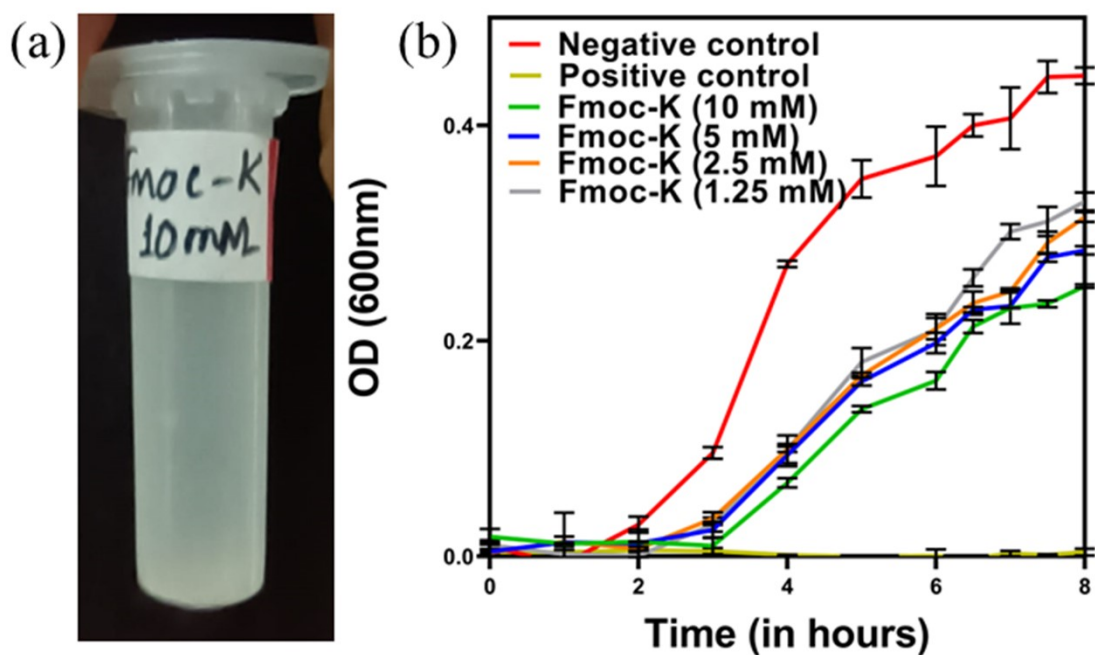


Figure S1. (a) Digital image of 10 mM Fmoc-K in 100 mM PB, after heating at 90°C followed by keeping it undisturbed for 24 hours, showing no gel formation and (b) Evaluation of the impact of Fmoc-K on the development of *E. coli* by turbidity measurement (absorbance values at 600 nm) with starting bacterial concentration was 10^5 CFU ml^{-1} . The growth kinetics data indicates that Fmoc-K shows similar anti-bacterial effect like Fmoc-F on *E. coli*.

(a)

Name of the samples	Concentrations (mM)	
	Fmoc-K	Fmoc-F
M1	5	10.0
M2	5	7.5
M3	5	5.0
M4	5	2.5
M5	5	1.25
M6	5	0.625
M7	5	0.3125

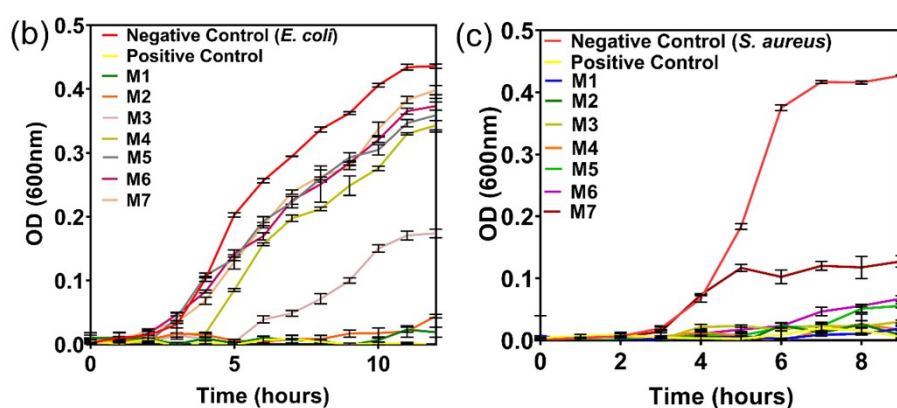


Figure S2. (a) Composition of Fmoc-K with varying concentrations of Fmoc-F (M1, M2, M3, M4, M5, M6 and M7). (b) Growth inhibition kinetics reflecting the effect of Fmoc-K with variable Fmoc-F concentrations on *E. coli*. (c) Growth inhibition kinetics with *S. aureus* in the presence of different compositions of Fmoc-K and Fmoc-F. Starting bacterial concentrations was 10^5 CFU ml^{-1} .

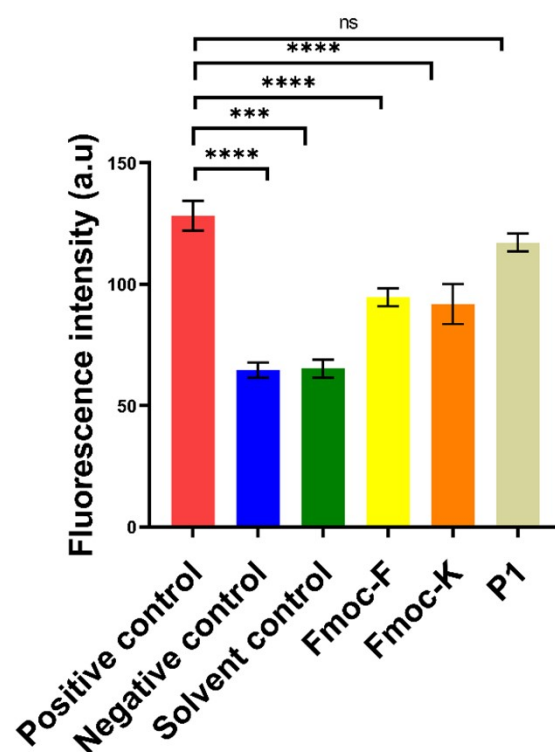


Figure S3. Effect of P1 and their components (Fmoc-F and Fmoc-K) on the Gram-positive bacterial membrane. The impact of Fmoc-F, Fmoc-K and P1 on the *S. aureus* membrane, evaluated by the use of a fluorescent hydrophobic dye, NPN, indicates higher fluorescence intensity for all the test agents representing their higher membrane permeability. The experiment performed thrice and the fluorescence intensity at 425nm (λ_{max}) plotted against the concentration of the test compounds gives P value < 0.001 when One way ANOVA, followed by Tukey test was performed to evaluate statistical significance.

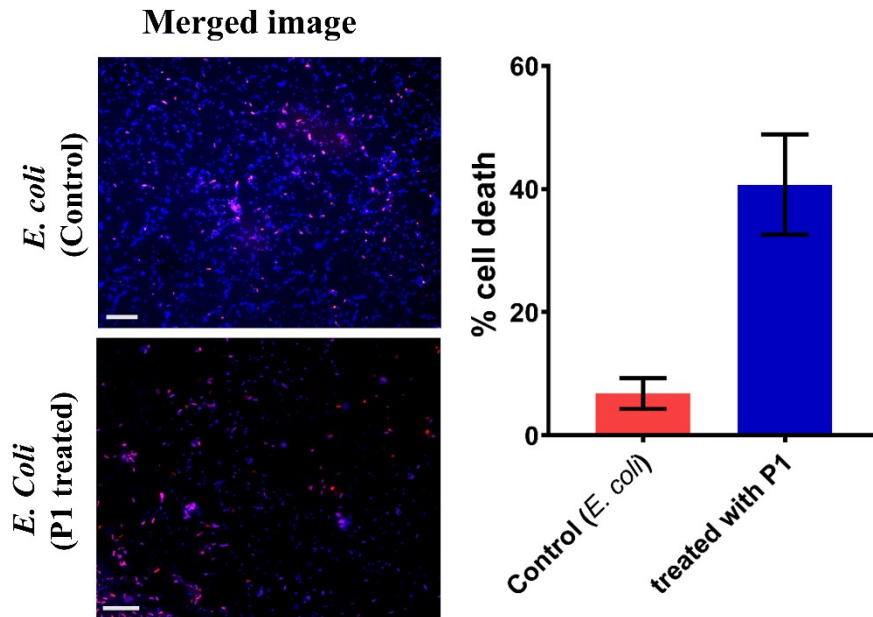


Figure S4. (a) Merged Fluorescence image (Blue fluorescence for DAPI and red fluorescence for PI) before and after treatment of *E. coli* with P1 (b) percentage cell death by counting the number of dead bacterial cells using ImageJ software, demonstrating higher proportion of cellular death after treatment with P1.

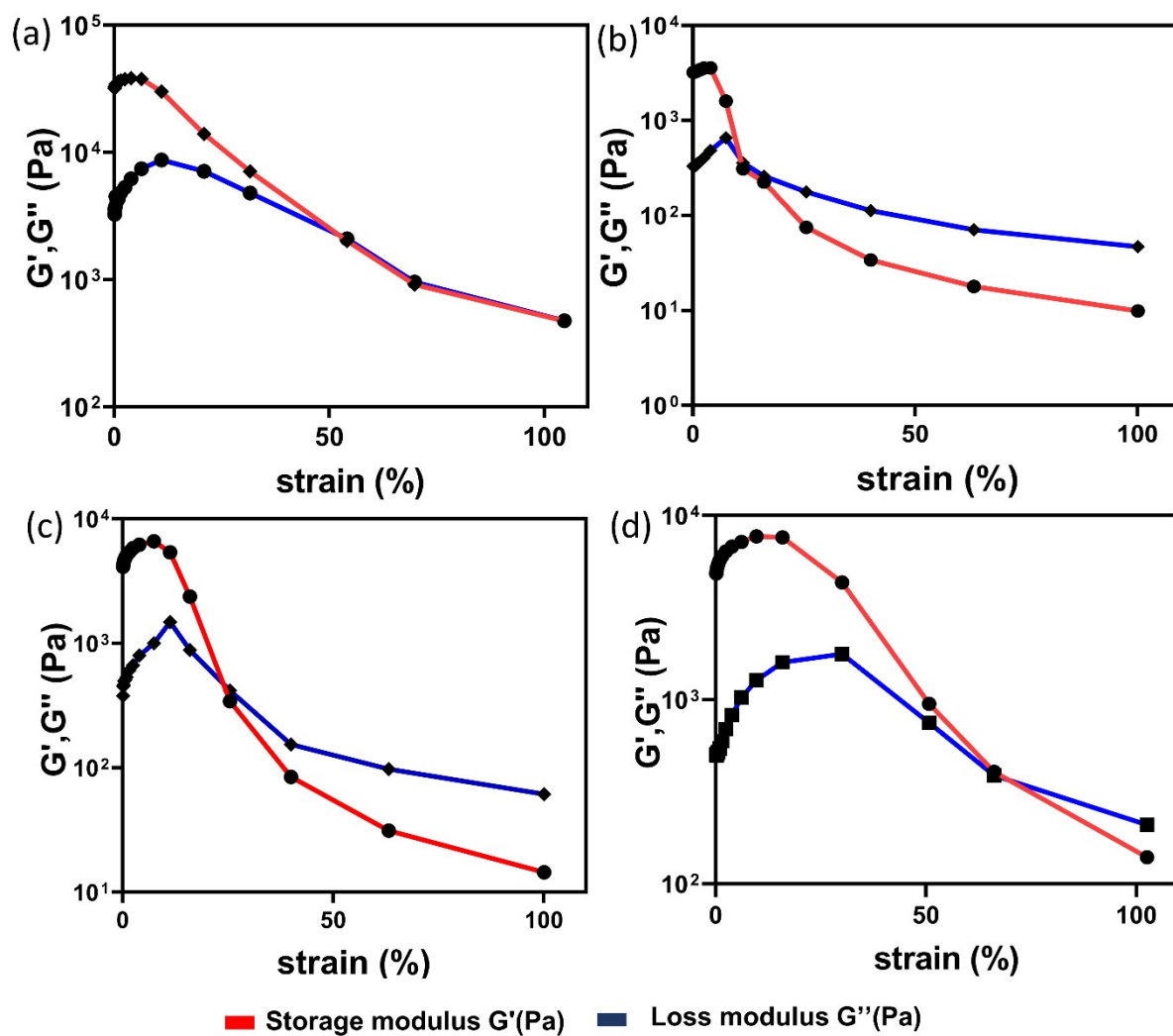


Figure S5. (a) Strain sweep tests at a constant applied frequency (0.1 Hz) for the self-assembled Fmoc-F and co-assembled composite gels P1 (b), P2 (c) and P3 (d) validate a broad linear viscoelastic regime (LVR).

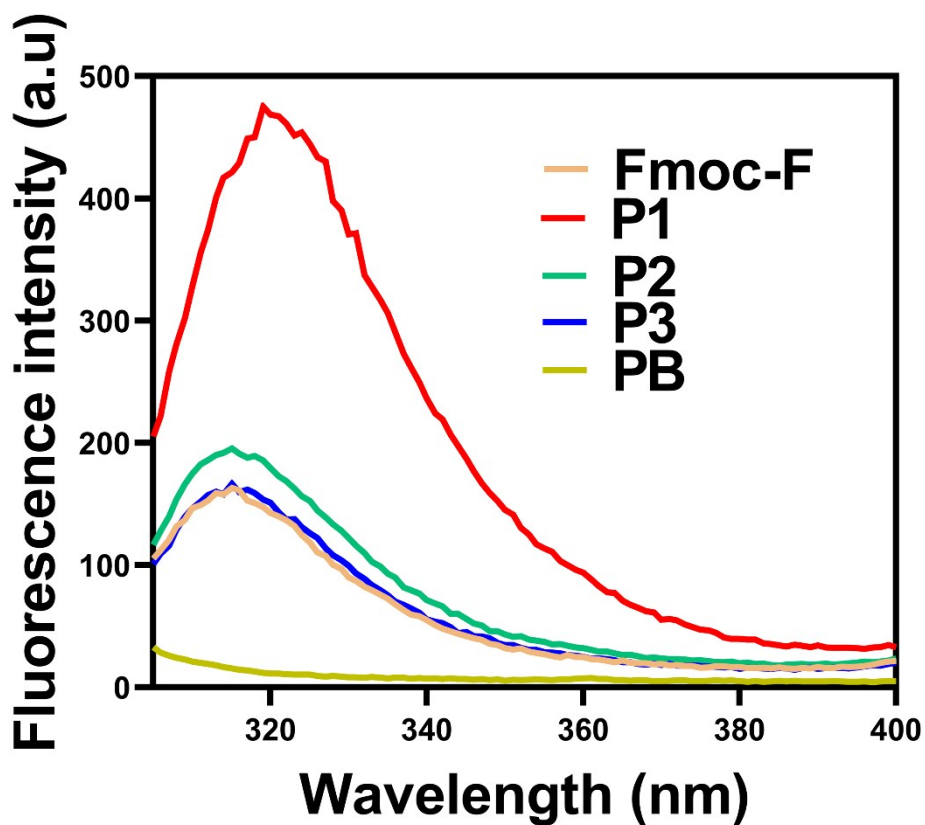


Figure S6. Fluorescence spectra of Fmoc-F, P1, P2 and P3. When excited at 296 nm, all the co-assembled hydrogels exhibit red-shift in fluorescence intensity as compared to Fmoc-F, demonstrating increased ' π - π ' interactions, resulting in higher stability. Also, the decreasing trend of this shift for these co-assembled hydrogels indicates that P1 has the highest stability followed by P2 and P3.

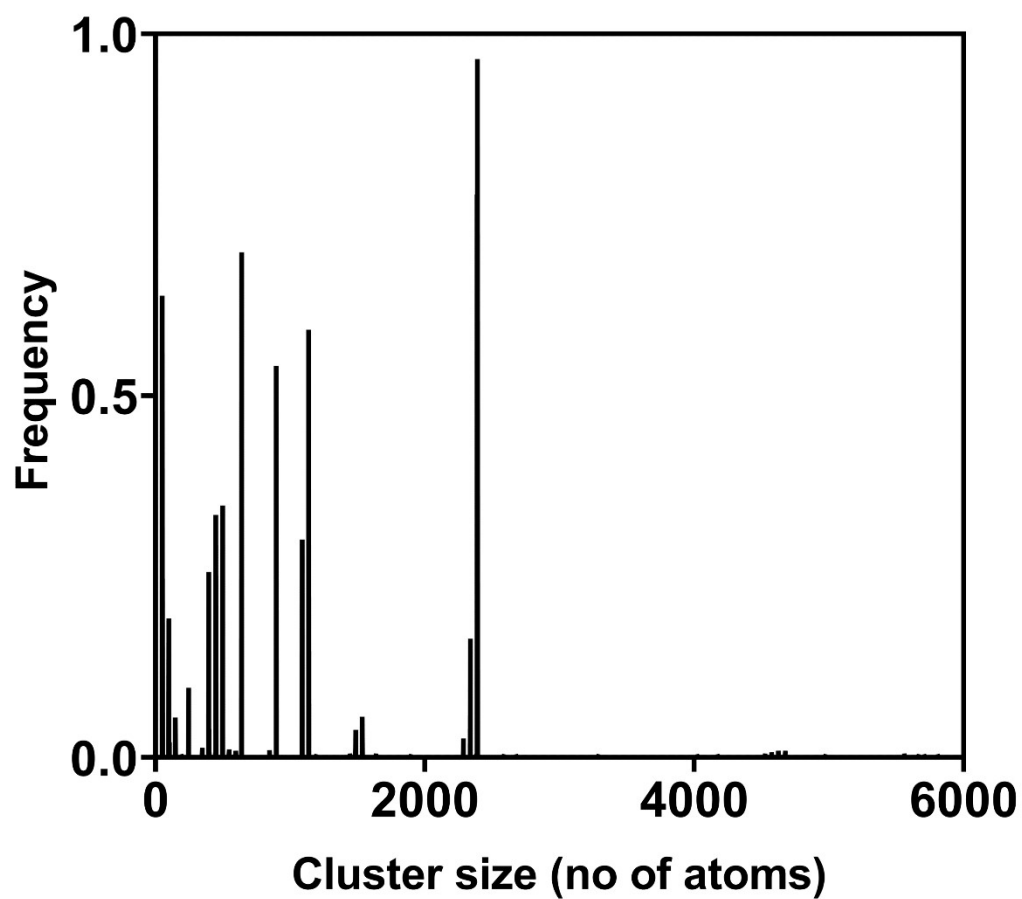


Figure S7. Distribution of sizes of the different clusters (number of atoms present in each cluster) and their frequencies as observed in MD simulation.

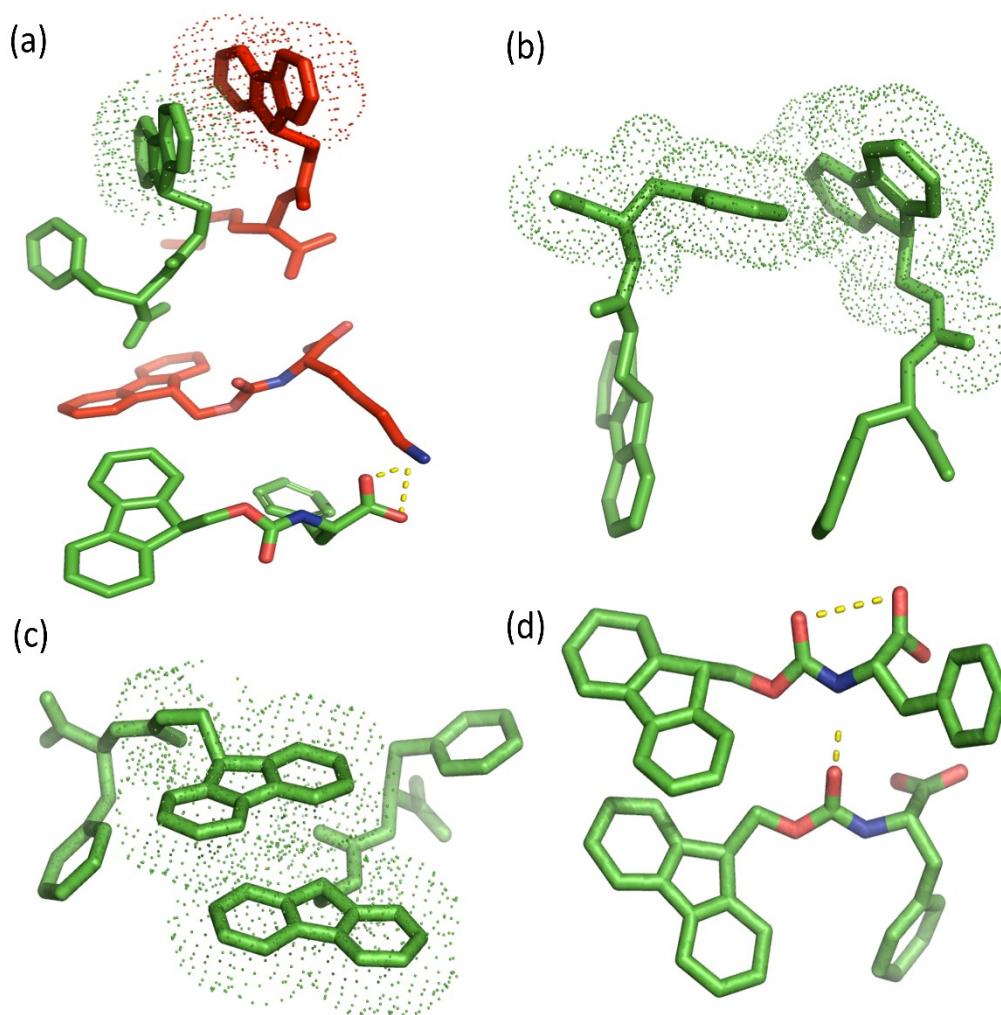


Figure S8. Snapshot of (a) π - π interaction and H-bonding/salt-bridge formation between Fmoc-K and Fmoc-F as observed in simulation. (b), (c), (d) π - π interaction and H-bonding between different molecules of Fmoc-F as observed in simulation.

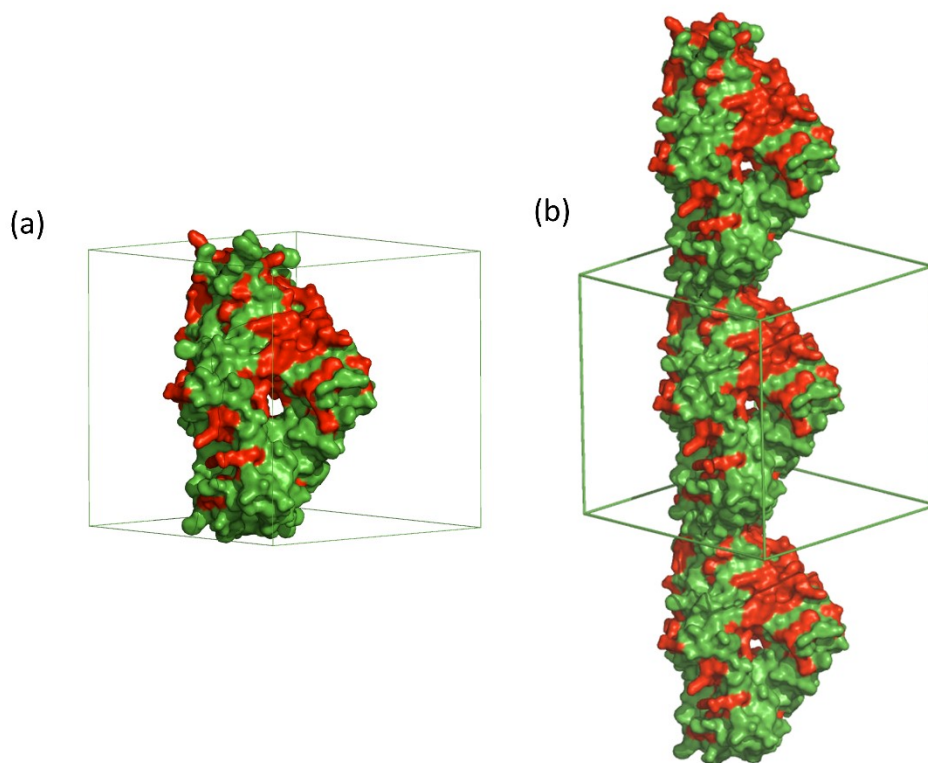


Figure S9. Snapshot of (a) a cluster and (b) a fiber lattice formed by the interactions between different molecules of Fmoc-F and Fmoc-K as observed at the final time frame of the simulation.

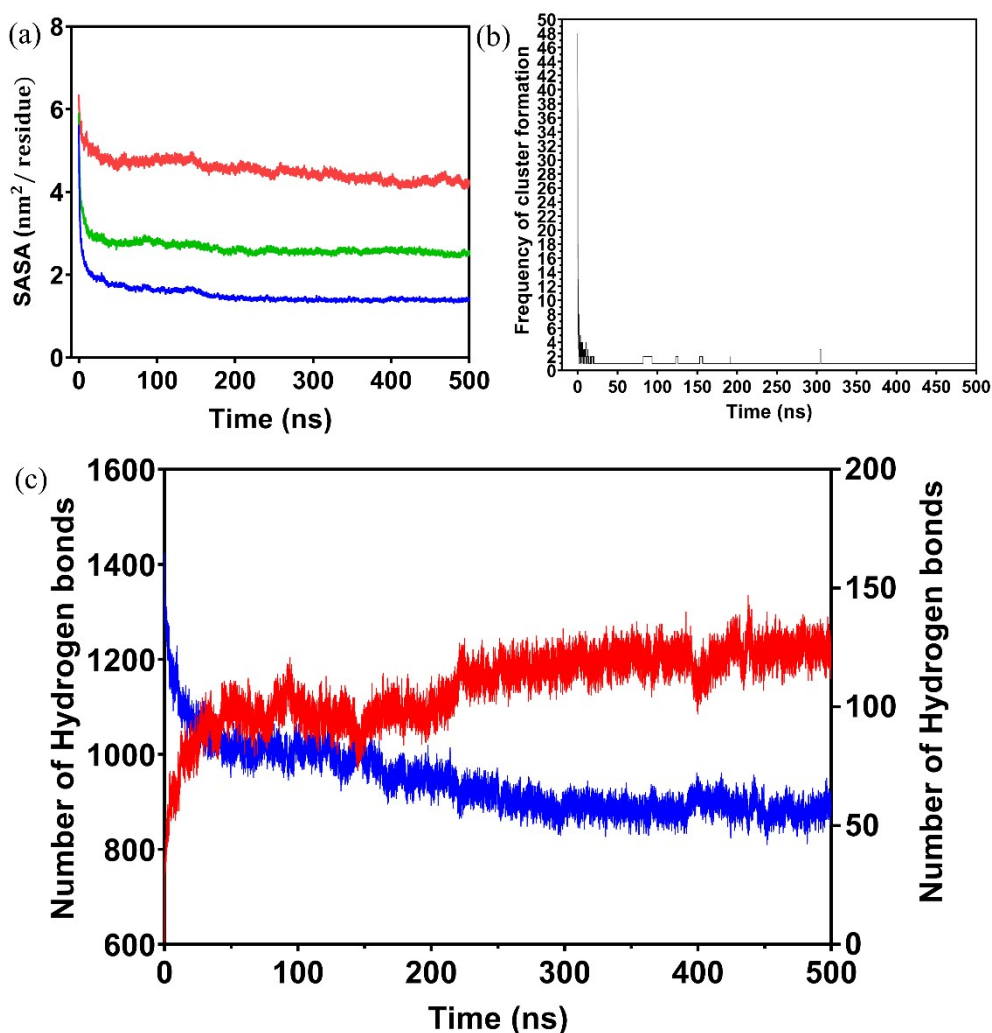


Figure S10. (a) Variation of solvent accessible surface area (SASA) of Fmoc-F (green) and Fmoc-K (red) and co-assembled system (blue) with simulation time. Convergence of SASA indicates a stable co-assembled system. (b) Variation of number of clusters as a function of simulation time. Number of clusters are much higher at the beginning of the simulation and converged to a fixed number of clusters at the end of the simulation. (c) Evolution of the number of H-bonds observed in the simulation process. The blue curve represents the H-bonding interaction between the amino acid conjugates and salts and waters present in the system. The red curve represents intermolecular and intramolecular H-bonding between Fmoc-K and Fmoc-F. H-bonding interactions between Fmoc-K/Fmoc-F increases over the simulation period with concomitant decrease in H-bonding between water/ions and solutes, a feature expected from the system undergoing self-assembly. The convergence of the number of H-bonding number around 300 ns indicated the stability of the system under simulation.

References

- 1 M. J. Abraham, T. Murtola, R. Schulz, S. Páll, J. C. Smith, B. Hess and E. Lindahl, *SoftwareX*, 2015, **1–2**, 19–25.
- 2 G. A. Kaminski, R. A. Friesner, J. Tirado-Rives and W. L. Jorgensen, *J. Phys. Chem. B*, 2001, **105**, 6474–6487.
- 3 W. L. Jorgensen, D. S. Maxwell and J. Tirado-Rives, *J. Am. Chem. Soc.*, 1996, **118**, 11225–11236.
- 4 S. Yuan, H. C. S. Chan and Z. Hu, *Wiley Interdiscip. Rev. Comput. Mol. Sci.* **2017**, 7 (2).
- 5 S. Rosignoli and A. Paiardini, *Biomolecules*, 2022, **12**, 1764.
- 6 X. Mu, K. M. Eckes, M. M. Nguyen, L. J. Suggs and P. Ren, *Biomacromolecules*, 2012, **13**, 3562–3571.
- 7 P. Mark and L. Nilsson, *J. Phys. Chem. A*, 2001, **105**, 9954–9960.
- 8 G. Bussi, D. Donadio and M. Parrinello, *J. Chem. Phys.*, **2007**, 126 (1).
- 9 M. Parrinello and A. Rahman, *J. Appl. Phys.* **1981**, 52 (12), 7182–7190.
- 10 M. A. Cuendet and W. F. van Gunsteren, *J. Chem. Phys.* **2007**, 127 (18).